

Seismic behavior of full-scale square concrete filled steel tubular columns under high and varied axial compressions

Hao D. Phan^{1a,2b} and Ker-Chun Lin^{*2c,3d}

¹Faculty of Civil Engineering, The University of Danang - University of Science and Technology, Danang 550000, Vietnam

²Department of Civil and Construction Engineering, National Taiwan University of Science and Technology, Taipei 10607, Taiwan

³National Center for Research on Earthquake Engineering, Taipei 10668, Taiwan

(Received December 30, 2019, Revised April 24, 2020, Accepted June 9, 2020)

Abstract. A building structural system of moment resisting frame (MRF) with concrete filled steel tubular (CFST) columns and wide flange H beams, is one of the most conveniently constructed structural systems. However, there were few studies on evaluating seismic performance of full-scale CFST columns under high axial compression. In addition, some existing famous design codes propose various limits of width-to-thickness ratio (B/t) for steel tubes of the ductile CFST composite members. This study was intended to investigate the seismic behavior of CFST columns under high axial load compression. Four full-scale square CFST column specimens with a B/t of 42 were carried out that were subjected to horizontal cyclic-reversal loads combined with constantly light, medium and high axial loads and with a linearly varied axial load, respectively. Test results revealed that shear strength and deformation capacity of the columns significantly decreased when the axial compression exceeded 0.35 times the nominal compression strength of a CFST column, P_0 . It was obvious that the higher the axial compression, the lower both the shear strength and deformation capacities were, and the earlier and faster the shear strength degradation occurred. It was found as well that higher axial compressions resulted in larger initial lateral stiffness and faster degradation of post-yield lateral stiffness. Meanwhile, the lower axial compressions led to better energy dissipation capacities with larger cumulative energy. Moreover, the study implied that under axial compressions greater than $0.35P_0$, the CFST column specimens with B/t limits recommended by AISC 360 (2016), ACI 318 (2014), AIJ (2008) and EC4 (2004) codes do not provide ultimate interstory drift ratio of more than 3% radian, and only the limit in ACI 318 (2014) code satisfies this requirement when axial compression does not exceed $0.35P_0$.

Keywords: concrete filled steel tubular (CFST) columns; seismic performance; axial compression; ultimate interstory drift ratio; B/t limit

1. Introduction

Compared to reinforced concrete (RC) as well as steel structural members, composite structural members possess excellent mechanical performance such as larger axial and lateral stiffness, greater compression and moment strengths, higher ductility, and better energy absorption capacity due to a proper combination of constitute materials: steel and concrete. It is clear that concrete filled steel tubular (CFST) columns significantly increase the loading capacity of the composite moment resisting frame (MRF) systems. In which, the steel tube helps to develop both column's moment resistance capacity and concrete confinement. On the other hand, the concrete core infill deters early local buckling occurring in the steel tube. Hence, it is possible to use a larger width-to-thickness ratio (B/t) of the steel tube in the CFST column than that in the pure steel column leading

to economy of steel material. In addition, outer steel tubes also play an important role as permanent formwork resulting in an easy and fast erection of buildings, therefore reducing both construction duration and cost (Uy 1998).

The seismic behavior of CFST columns varies according to several factors such as shape and dimension of the cross-sections, steel tube thickness, material properties, steel-concrete interaction condition, and axial compression level. A study conducted on circular filled composite columns by Boyd *et al.* (1995) showed that thicker steel shell of tube and shear studs resulted in higher strength and better energy dissipation capacity of the column. Additionally, it was revealed that when higher strength concrete was used, stronger ultimate strength was obtained but more rapid strength degradation and lower energy dissipation were observed. Another study (Fam *et al.* 2004) pointed out that flexural strength and ductility of circular CFST columns were not significantly influenced by different bonding and end loading conditions. Han *et al.* (2003) studied seismic behavior of square and rectangular CFST (thin-walled) columns and concluded that increasing axial compression level, slenderness ratio, and concrete strength decreased the column ductility. In contrast, the column ductility became higher by increasing the steel ratio. In addition, several remarkable studies on circular/square CFST columns using

*Corresponding author, Ph.D. Professor

E-mail: kclin@ncrec.narl.org.tw

^aSenior Lecturer

^bPh.D. Scholar

^cProfessor

^dResearch Fellow

high strength materials were conducted (Fujimoto *et al.* 2004, Inai *et al.* 2004, Varma *et al.* 2002a, 2002b, Varma *et al.* 2004, Varma *et al.* 2005). In Fujimoto *et al.*'s (2004) study on circular CFST columns under eccentric loading, the use of high strength concrete led to a reduction of column ductility. By contrast, the use of high strength steel or a low diameter-to-thickness ratio (D/t) resulted in an increase of column ductility due to the concrete confinement effect. However, for square CFST columns, the confinement effect was smaller than in circular ones, and the local buckling phenomenon occurred early in the steel tubes with a larger width-to-thickness ratio (B/t). Moreover, their research had done numerical analysis using fiber elements and considered the effects of member size, concrete confinement and tube wall's local buckling on these CFST columns' performances. The seismic behavior of both circular and square CFST columns using high strength materials was also investigated by Inai *et al.* (2004). They pointed out that circular CFST columns showed greater ductility and higher moment resistance than square ones due to better concrete confinement from the round steel tube. The increase of B/t also reduced the ductility of square CFST columns. The increasingly varied axial load led to a column ductility reduction due to premature local buckling concentrated in one of two flanges. Varma *et al.* (2002a, 2002b, 2004, 2005) investigated the effects of high material strengths in steel and concrete, B/t and axial compression levels on seismic performance of square CFST columns. Their results showed that flexural stiffness and moment strength of these columns were insignificantly influenced by loading types such as monotonic or cyclic, but the post-peak moment resistance reduced rapidly in the case of latter loading type. It also was pointed out that cyclic-reversal load resulted in a decrease of flexural stiffness of the composite column. In general, increasing B/t and axial compression levels decreased cyclic curvature ductility of the CFST columns. At the axial compression level of 10% of the column's nominal compressive strength, P_0 , increasing steel grade or B/t significantly decreased cyclic curvature ductility, but at the axial compression level of $0.2P_0$, it had insignificantly influenced on cyclic curvature ductility.

Besides, the limit values of B/t or D/t for designing composite columns are different according to not only the current design codes of AISC 360 (2016), ACI 318 (2014), AIJ (2008) and EC4 (2004) but also the seismic codes of AISC 341 (2016) and EC8 (2004). The shortage of past studies was that there has been no recommendation on the upper limit of axial compression for CFST columns. The limit of B/t for CFST columns under high axial compression must be investigated for columns in lower stories of building located in high seismic zones.

From the literature reviews mentioned above, some research gaps in understanding the real seismic performance of square CFST column members in the buildings located in high seismic zones, as shown below.

(a) There is a lack of seismic experimental results of full-scale square CFST columns under high axial compression (Thai *et al.* 2019).

(b) The seismic behavior of an exterior column in the

MRF system has not been investigated adequately. In fact, the exterior columns in lower building stories are subjected to varied axial load under seismic conditions. Thus, it is necessary to use a varied axial loading protocol to conduct testing.

(c) B/t limits required in these current design codes are different. Furthermore, the limit of B/t recommended in these codes without considering the influence of axial compression may not be reasonable, so it needs to be further investigated.

The common use of composite members in constructions, together with the complexity of earthquakes occurring in the world, has motivated research projects on seismic performance evaluations of composite members under earthquake loading. The National Center for Research on Earthquake Engineering (NCREE) in Taiwan is an excellent place with sufficient facilities to investigate these research topics. Hence, this study investigates the seismic performance of full-scale square CFST columns under various axial compression levels and types, especially high axial compression. Experimental behaviors and the influences of research variables on strength and deformation capacity, strength degradation, lateral stiffness degradation, and energy dissipation capacity of these CFST columns are presented in detail.

2. Experimental program

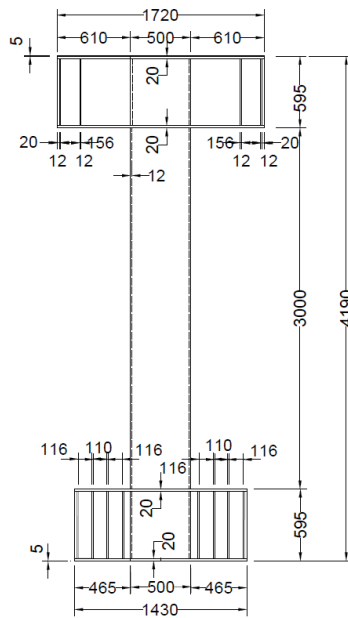
This research project includes both parts of experimental investigation and numerical analysis. In the first part, an experimental program was made to test four full-scale square CFST column specimens subjected to axial and lateral loads. This paper presents the obtained results of the first part. The main research parameter considered in this paper is the axial compression level and type that contain three constant axial compression levels and one varied axial compression type. A width-to-thickness ratio of steel tube, B/t , of 41.7 (rounded to 42) is designed for all four specimens. The test matrix of all specimens is presented in Table 1. Herein, the symbol CFST42-35C illustrates a CFST column specimen with B/t of 42 and subjected to a constant axial compression of $0.35P_0$. The symbol CFST42-15/55C illustrates a specimen with B/t of 42 and subjected to a variable axial compression ranging from 0.15 to $0.55P_0$.

2.1 Specimen design

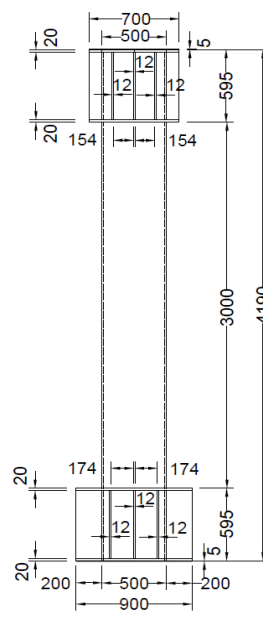
As shown in Table 1 and Fig. 1, the four specimens' dimensions and steel material were identical. SN 490B steel plate, $f_y = 345$ MPa, with its thickness of 12 mm was used. Square tube's outer width B was equal to 500 mm and its corners were bent with an inner and outer radius of 18 and 30 mm, respectively. The steel tube was made of two U-shape components using complete joint penetration (CJP) groove welds. Top and bottom footings consist of steel plates of 12 and 20 mm thickness welded together. The steel tube was penetrated the two footings. The total height of the specimen and the column clearance height (L) are 4.2 and 3.0 m, respectively. The B/t limits provided by the current

Table 1 Test matrix of CFST column specimens

Specimen	$B \times t \times L$ (mm)	L/B	B/t	b/t	f_y (MPa)	f_{ya} (MPa)	f'_c (MPa)	f'_{ca} (MPa)	P/P_0
CFST42-15C	500x12x3000	6	41.7	36.7	345	351	35	35.3	0.15
CFST42-35C	500x12x3000	6	41.7	36.7	345	351	35	37.7	0.35
CFST42-55C	500x12x3000	6	41.7	36.7	345	351	35	35.5	0.55
CFST42-15/55C	500x12x3000	6	41.7	36.7	345	351	35	36.9	0.15-0.55



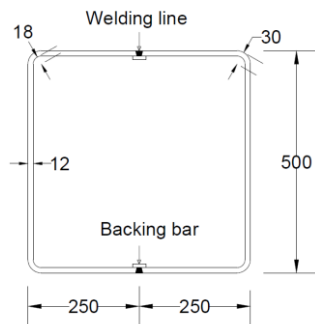
(a) The front view



(b) The side view



(c) Completed specimens



(d) Steel tube cross-section



(e) A completed steel tube

Fig. 1 Dimensions and details of specimens (units: mm)

design codes including AISC 360 (2016), AISC 341 (2016), ACI 318 (2014), AIJ (2008), EC4 (2004) and EC8 (2004) are shown in Table 2. In this study, the 42 of B/t was chosen from the ACI 318 (2014) code (see Tables 1 and 2). This value also satisfies the requirements in AISC 360 (2016), AIJ (2008) and EC4 (2004) codes, but does not satisfy those in AISC 341 (2016) and EC8 (2004) codes.

2.2 Material properties

2.2.1 Plate steel for tubes

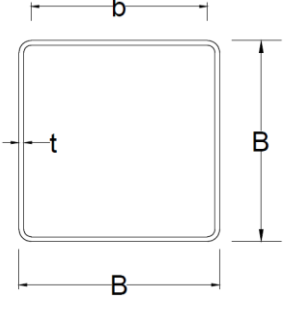
Tensile tests of SN 490B steel plates were conducted according to the ASTM E8/E8M (2008) standard. Actual steel mechanical properties were defined by average values obtained from three tensile coupon specimens. These

include actual yield stress $f_{ya} = 351$ MPa, ultimate stress $f_{ua} = 518.4$ MPa, yield strain $\epsilon_y = 0.00175$ and ultimate strain $\epsilon_u = 0.1542$.

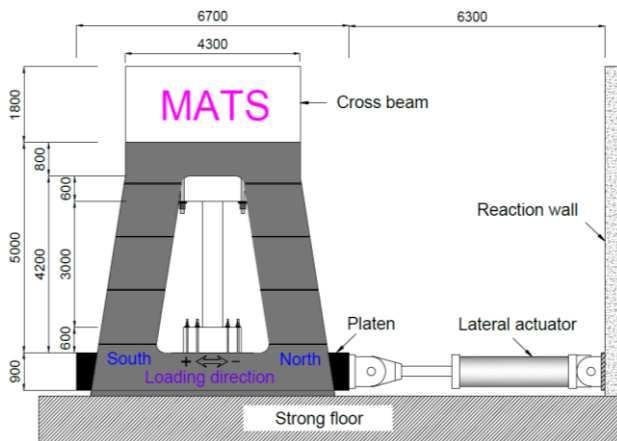
2.2.2 Infilled concrete

The design compressive strength of concrete was equal to 35 MPa. To eliminate the shrinkage effect of concrete in the steel tube, fresh concrete was filled into the steel tube up to a level below the inner surface of the top plate 20 mm. After that, mortar with high strength of 56 MPa was filled into these remaining spaces. Fifteen concrete cylinder samples ($D = 150$ mm and $H = 300$ mm) were made and cured in the non-water condition as same as the column specimens. In which, first three concrete cylinders were tested at the age of 28 days. For other concrete cylinders,

Table 2 Width-to-thickness ratio (B/t) limitations

Design code	The square hollow section	B/t (or b/t) limits	Code-allowable B/t	
			$(f_y = 345 \text{ MPa})$	$(f_{ya} = 351 \text{ MPa})$
AISC 360 (2016)		$\frac{b}{t} \leq 2.26 \sqrt{\frac{E_s}{f_y}}$	57.4	57.0
AISC 341 (2016)		$\frac{b}{t} \leq 1.48 \sqrt{\frac{E_s}{R_y f_y}}$	34.0	33.7
ACI 318 (2014)		$\frac{B}{t} \leq \sqrt{\frac{3E_s}{f_y}}$	41.7	41.4
AIJ (2008)		$\frac{B}{t} \leq 2.47 \sqrt{\frac{E_s}{f_y}}$	59.5	59.0
EC4 (2004)		$\frac{B}{t} \leq 52 \sqrt{\frac{235}{f_y}}$	42.9	42.6
EC8 (2004)		$\frac{B}{t} \leq 24 \sqrt{\frac{235}{f_y}}$	19.8*	19.6*

*This value required in dissipative zones of highly ductile members



(a) Schematic of the test setup (units: mm)



(b) Photo of the test setup

Fig. 2 Test setup for a CFST column specimen on the MATS

each group of three samples was tested on the same day of each CFST column specimen's testing. Actual compressive strengths for four specimens obtained from uniaxial compression tests are shown in Table 1.

2.3 Testing procedure

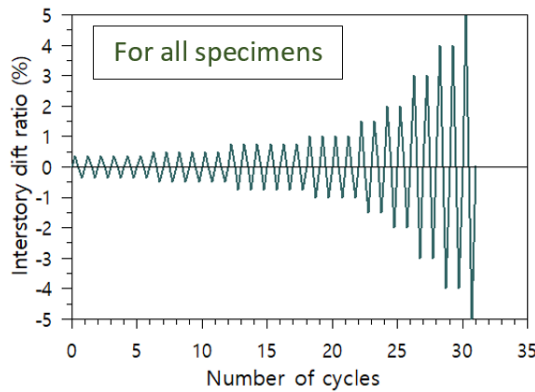
2.3.1 Test setup

The Multi-Axial Testing System (MATS) facility at NCREC was used for testing. The test setup for a CFST column specimen is shown in Fig. 2. A procedure of assembling the specimen on the MATS: Firstly, the specimen was lifted and put on the platen. This platen was connected with a horizontal loading system of two parallel actuators providing specimen's cyclic lateral displacement loading. The axially compressive force to the specimen was applied by seven vertical actuators of MATS placed underneath the platen. Then the specimen's bottom and top footings were fixed to the platen and the top cross beam

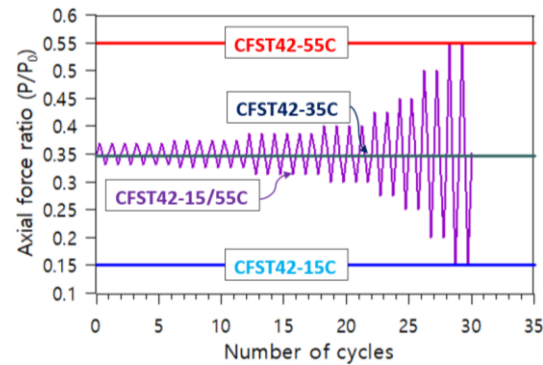
MATS by high strength steel rods, respectively. To increase friction forces between the specimen and surfaces of the cross beam and the platen, the two interfaces were inserted by two 5-mm aluminum plates. Secondly, to measure local displacements on the steel tube surfaces, two NDI machines were set up on the eastern and western sides. On each side, a total of thirty-four NDI makers was attached and connected to a computer. Thirdly, to measure the strain of the steel tube, sixty-seven strain gauges were connected to another control computer. Fourthly, to measure relatively lateral displacement between two ends of the column, two Tempos were installed (see Fig. 2(b)). Finally, to capture global pictures on four sides of the column during the test, four cameras were set up.

2.3.2 Loading protocols

In the four specimens, three ones were subjected to constant axial compressions of 0.15, 0.35 and 0.55 P_0 , respectively, combined with cyclic-reversal lateral displacement



(a) Cyclic-reversal lateral displacement loading protocol (AISC 341 (2016) code)



(b) Constant and varied axial compression loading protocol

Fig. 3 Loading protocols for seismic testing

according to the AISC 341 (2016) code. The remaining specimen was subjected to varied compression ranging from $0.15P_0$ to $0.55P_0$ (corresponding to the interstory drift ratio ranging from -4% to $+4\%$ radian), $0.35P_0$ was a middle value (at 'zero' interstory drift ratio), combined with the lateral displacement mentioned above, as shown in Fig. 3. Herein, Fig. 3(a) depicts lateral displacement simulating earthquake load. It is divided into several steps with a various number of cycles and amplitudes of interstory drift ratio. In which, six cycles are specified in the first three loading levels with interstory drift ratios of 0.375 , 0.5 , and 0.75% radian, respectively. There are four cycles at 1% and two cycles at 1.5% radian of the interstory drift ratio. Then, from 2% , radian and more, two cycles are used with an increment of 1% radian. Fig. 3(b) shows three levels of the constant axial compression and the varied axial compressive load. The arrangement of the compressive loads in this research assumed that the middle interior column of a typical MRF system normally subjected to axial compression around $0.35P_0$ from gravity loads. The two exterior columns on both sides of the frame subjected to less and more axial compression than the interior one, respectively, under earthquake action. Therefore, for the last specimen (CFST42-15/55C), initial axial compression of $0.35P_0$ was applied. Then, the axial compression was proportionally changed as same as the frequency of lateral displacement. The varying amount of axial compression is to plus or minus $0.05P_0$ when increasing or decreasing 1% radian of interstory drift ratio, respectively.

3. Test results and experimental analyses

3.1 Experimental behavior

Generally, the critical deformation or fracture of all specimens occurred at the column ends within a distance of around B from the footings. The significant deformation of the column happened within a distance between $B/4$ and $B/2$ from the ends of the column. Test observations were found some important discrepancies in this experiment between the four specimens as below.

Specimen CFST42-15C was tested under a combination of the lowest constant axial compression ($0.15P_0$) and cyclic lateral loading. Fig. 4 depicts deformation and fracture at the top and bottom ends of the column at interstory drift ratios of 1.5% , 2% , 3% and 5% radian, respectively. Firstly, the steel tube yielding occurred at an interstory drift ratio of 1% and widely spread at 1.5% radian. Then, local buckling occurred in flanges and webs at the final cycle of 2% and 3% , respectively. Next, at the 5% drift ratio, severe local buckling dramatically developed in webs. At this moment, cracks at steel tube corners and crushed concrete inside were found. Finally, the specimen was observed severer buckling and larger cracking fractures in the steel tube and concrete crushing more intensive at the drift ratio of 6% . It was found that the buckling position was located in webs nearer to the footings than in the flanges. This may be caused by low axial compression.

Specimen CFST42-35C was tested under a medium constant axial compression, $0.35P_0$, in conjunction with cyclic lateral loading. Deformation and fracture at the top and bottom ends of the column at interstory drift ratios of 1% , 1.5% , 2% , and 3% radian, respectively, are shown in Fig. 5. Firstly, at an interstory drift ratio of 0.75% radian, the steel tube started yielding in its flanges. Then, steel yielding spread wider in flanges and webs at the drift ratio of 1% and 1.5% , respectively. The commencement of local buckling occurred in flanges after finishing the drift ratio of 2% . Next, at the drift ratio of 3% , larger local buckling happened in flanges and developed significantly in webs. Finally, an important event happened in the first cycle of the drift ratio of 4% . The constant axial compression applied during the test was not remained and the shear was lower than 80% of its maximum testing shear. Hence, for evaluating the seismic performance of Specimen CFST42-35C, it can be concluded this specimen failed at the interstory drift ratio of 4% .

Specimen CFST42-55C was tested under the highest constant axial compression, $0.55P_0$, combined with cyclic lateral loading. Fig. 6 depicts deformation and fracture at the top and bottom ends of the column at interstory drift ratios of 0.75% , 1% , and 1.5% radian, respectively. Firstly, the yielding started and spread wider in the steel tube at the

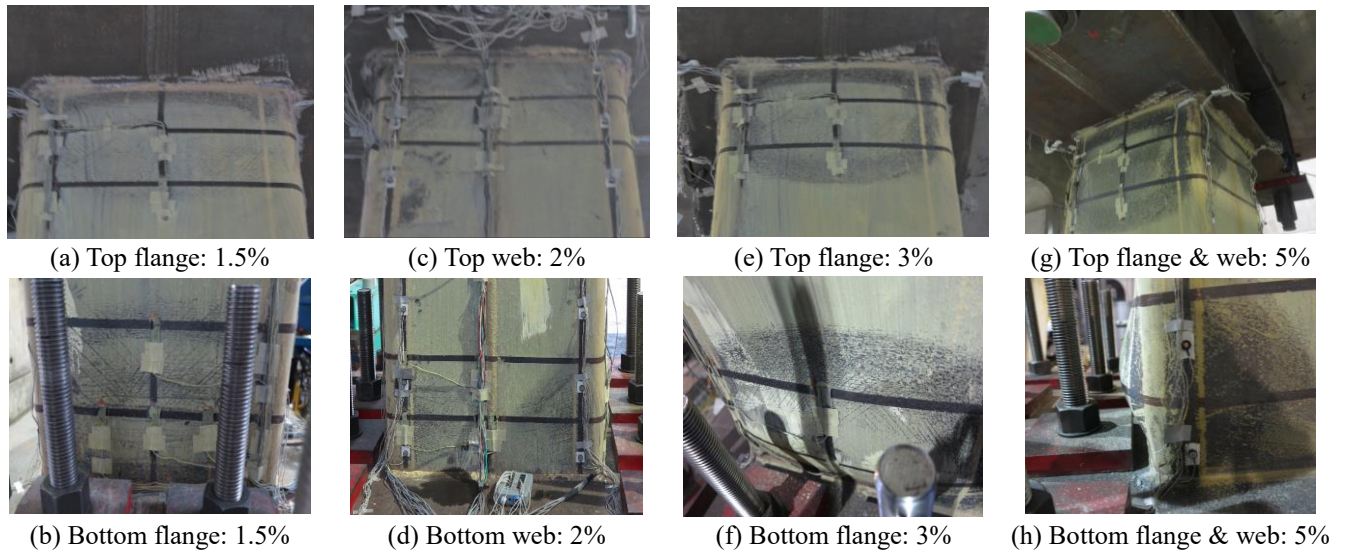


Fig. 4 Deformation and fracture stages of Specimen CFST42-15C

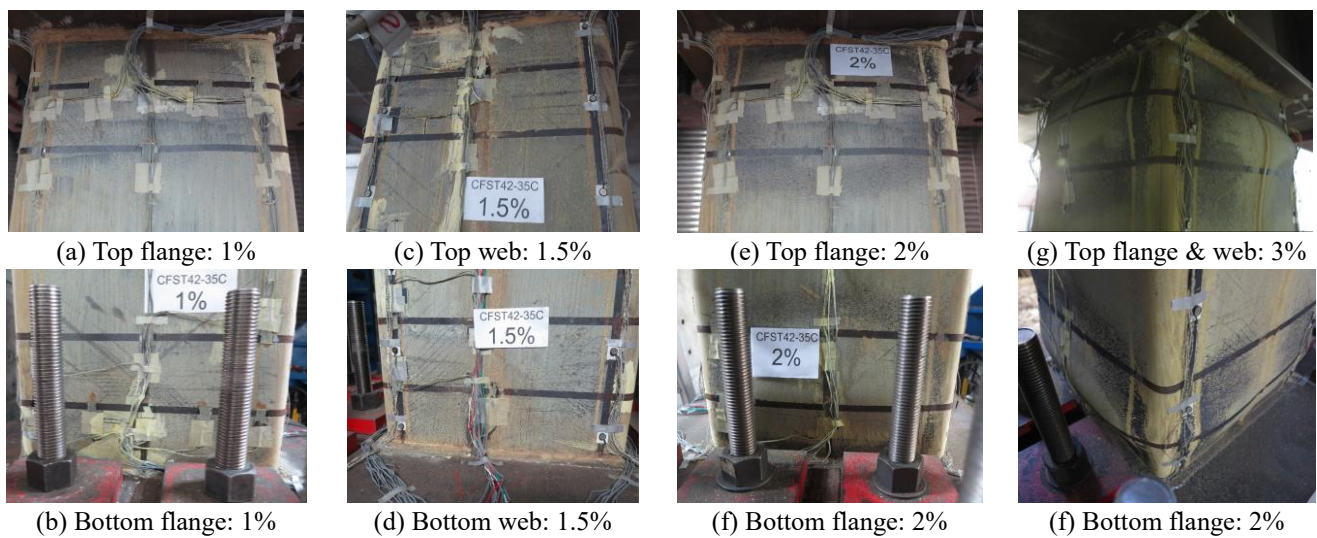


Fig. 5 Deformation and failure stages of Specimen CFST42-35C

drift ratio of 0.5% and 0.75% radian, respectively. Then, local buckling occurred and developed in flanges and webs during the four cycles of the drift ratio of 1%. Next, at the drift ratio of 1.5%, local buckling quickly developed in flanges and webs due to the effect of high axial compression. Finally, the constant axial compression applied during the test was not remained and the shear was lower than 80% of its maximum testing shear at the beginning of the first cycle of the 2% drift ratio. In summary, this specimen failed at 1.5% radian that lower than the two previous specimens.

Specimen CFST42-15/55C was tested under varied axial compression in conjunction with cyclic lateral loading. Deformation and fracture at the top and bottom ends of the column at interstory drift ratios of 1%, 1.5%, 2%, and 3% radian, respectively, are shown in Fig. 7. Firstly, yielding started in the steel tube at the drift ratio of 0.75% and developed at 1% radian in the positive direction of lateral displacement. Then, steel yielding spread wider in flanges and webs at the drift ratio of 1.5%. Next, local buckling

started in flanges at around 2%. At the drift ratio of 3%, local buckling developed in flanges and webs. In which, an interesting finding is that buckling in webs was asymmetrical in the positive and negative directions and then full buckling spread to the entire web in the first cycle. This entire buckling in webs developed severer in the second cycle. Finally, the negative response, that the testing axial compressive load was not able to keep at the specified value, was found at the beginning of the 4% drift ratio. This means that the varied axial compression changing up to from 0.2 to $0.5P_0$, corresponding to the interstory drift ratio from -3% to $+3\%$, respectively, could be maintained (see Fig. 3(b)), but the column failed with increasing axial compression up to $0.55P_0$. Hence, for evaluating the seismic performance of Specimen CFST42-15/55C, it can be concluded this specimen failed at the drift ratio of 3% radian in the positive direction.

After removing the steel walls near the column bottom ends of Specimens CFST42-15C and CFST42-55C, crushes and cracks of the inner crushed concretes were observed

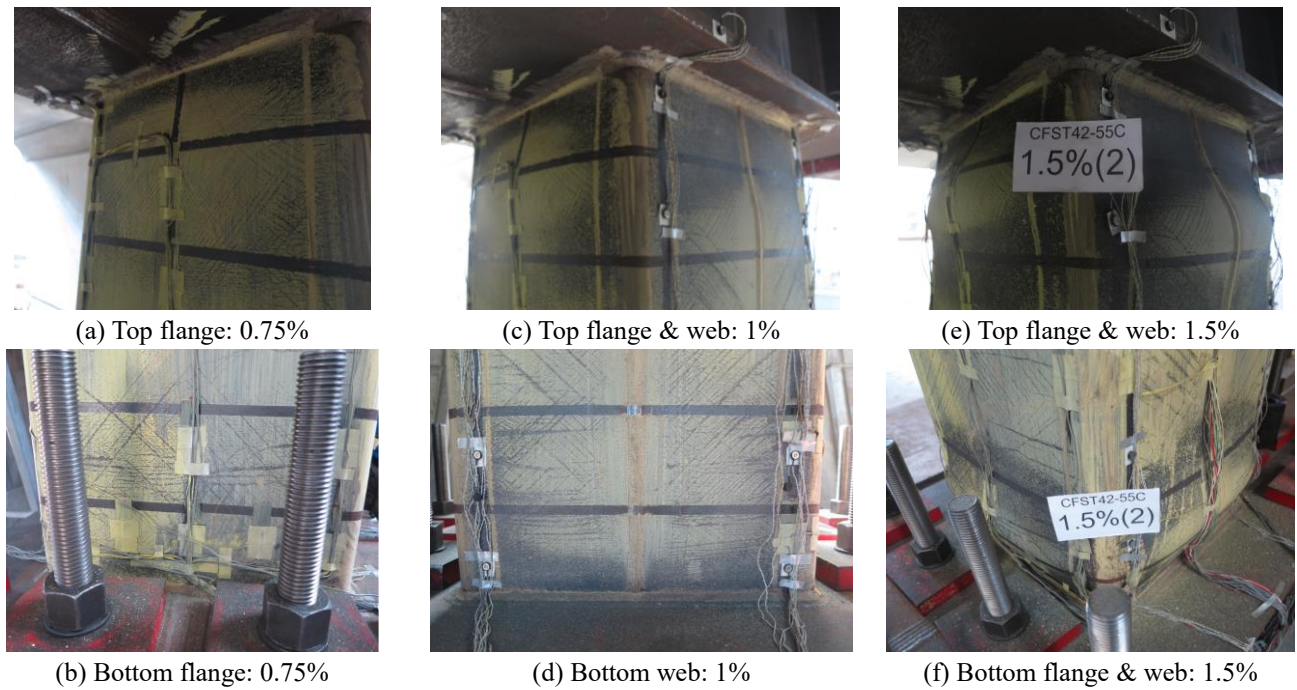


Fig. 6 Deformation and failure stages of Specimen CFST42-55C

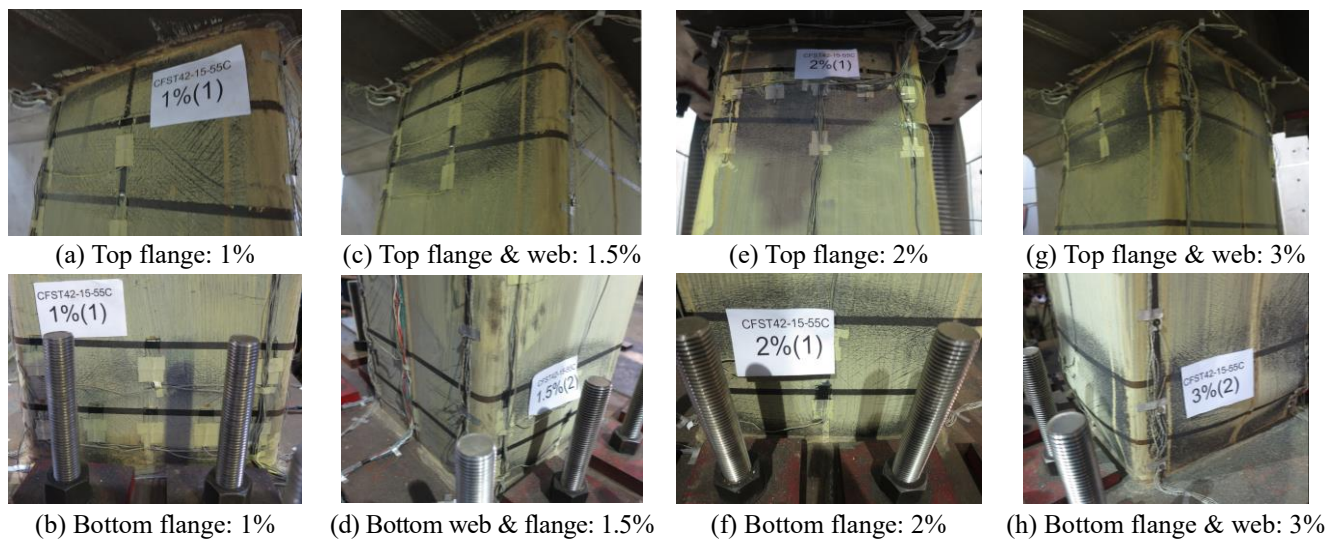


Fig. 7 Deformation and failure stages of Specimen CFST42-15/55C

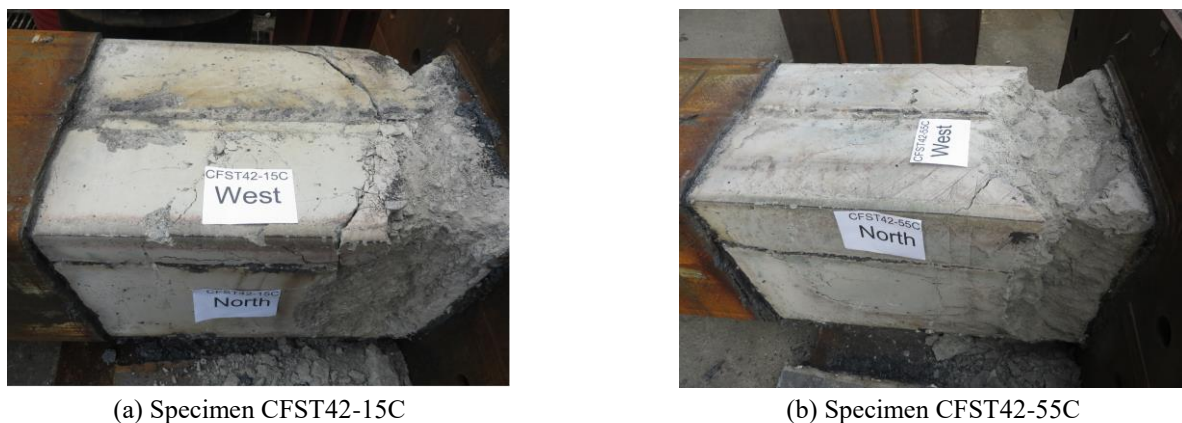


Fig. 8 Crushed concrete at the column's bottom end

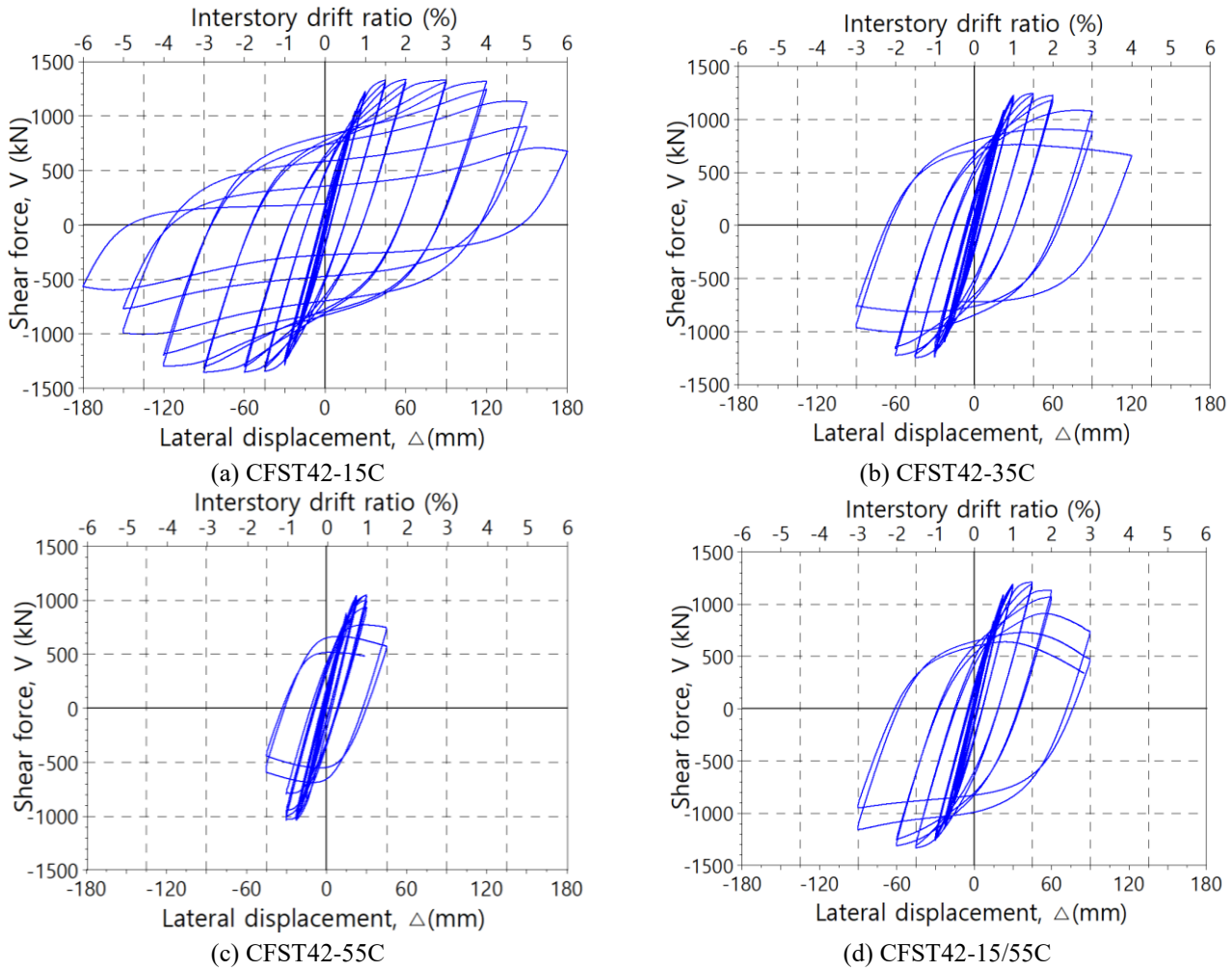


Fig. 9 Shear force - lateral displacement ($V-\Delta$) hysteresis loops

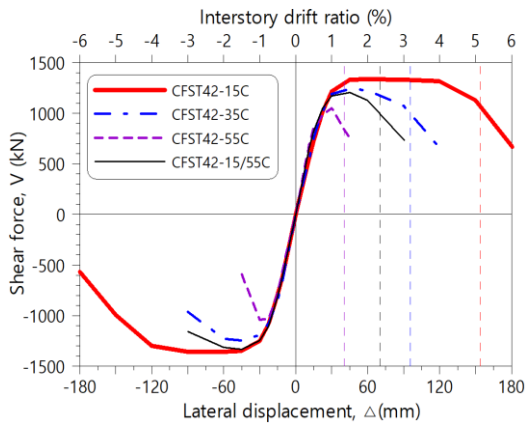


Fig. 10 Comparisons of cyclic response envelopes

clearly in Fig. 8. Concrete crushing appeared adjacent to the outward local buckling positions of the steel tube. The observations from the crushed concrete (Fig. 8) show that for the Specimen CFST42-15C subjected to lower axial compression, the concrete crushing was wider and deeper on the flange sides than that on the web sides. However, for the Specimen CFST42-55C with higher axial compression, a little wider and deeper concrete crushing occurred on both flange and web sides. Also, it reveals that for the specimen

with higher axial compression (CFST42-55C), the concrete cracks were steeper than that for Specimen CFST42-15C with lower axial compression.

3.2 Shear force versus lateral displacement responses

Shear force vs lateral displacement ($V-\Delta$) hysteresis loops of four specimens are shown in Fig. 9. These hysteresis loops reveal that the axial compression significantly affected the performance of the CFST columns to cause that the higher the axial compression, the poorer the capacity of lateral displacement. This influence is similar to the results of Zhang *et al.* (2007). Specimen CFST42-15C having the lowest constant axial compression performs the highest strength and the best deformation capacity to compare to the others. As shown in Fig. 9(a), this column sustained a high capacity almost to the drift ratio of 4% radian and degraded from 5%. Specimens CFST42-35C and CFST42-55C tested with higher constant axial compression, the lateral strengths degraded and the capacities of lateral deformation reduced significantly to 3% and 1.5% radian, respectively. Based on the results of the three specimens subjected to constant axial

Table 3 Test results of four specimens

Specimen	DR _{max} (%)	V _{max} (kN)		Δ_u at 0.8V _{max} (mm)		DR _u at 0.8V _{max} (%)	
		Pos./Neg.	Average	Pos./Neg.	Average	Pos./Neg.	Average
CFST42-15C	(+)	2.0	1337	153.9	147.5	5.13	4.92
	(-)	2.0	1357	141.0		4.70	
CFST42-35C	(+)	1.5	1244	95.7	90.9	3.19	3.03
	(-)	1.5	1249	86.1		2.87	
CFST42-55C	(+)	1.0	1051	40.5	38.7	1.35	1.29
	(-)	1.0	1041	36.9		1.23	
CFST42-15/55C	(+)	1.5	1208	70.2	-	2.34	-
	(-)	1.5	1334	90.0+	-	3.00+	-

DR_{max}: Interstory drift ratio corresponding at the maximum shear force (V_{max}); Δ_u and DR_u: Ultimate lateral displacement and interstory drift ratio that corresponding at 0.8V_{max} beyond the peak value; Pos./Neg.: Values in positive and negative directions

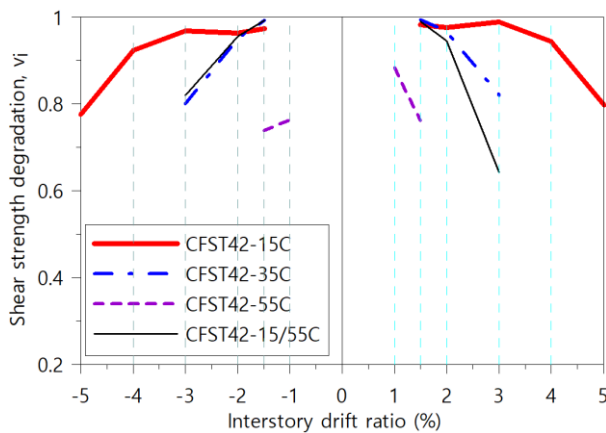


Fig. 11 Comparisons of shear strength degradation

compressions, the higher the axial compression, the more significant degradation of shear strength was, for instance, Specimen CFST42-55C was the worst seismic performance column (see Fig. 9(c)). Moreover, the varied pattern of axial compression caused asymmetrical behavior in Specimen CFST42-15/55C, as shown in Fig. 9(d). It is found that the shear response in the negative direction (decreasing axial compression) was larger than that in the positive direction (increasing axial compression). With a comparison of the shear degradation ratios of 3% to 1.5% radian of the interstory drift ratio in the two directions, the degradation ratio being 0.612 in the positive direction was more serious than 0.869 in the negative direction. Besides, there was a pinching effect to be found in Fig. 9 for all four specimens. This pinching effect of the CFST columns mainly resulted from buckling in the steel wall and cracking or crushing on the internal concrete under cyclic loading. This was because that when the latter unloading and applying toward the opposite direction were done, the buckled steel wall and the cracked and crushed concrete were merely restored by less stiffness and strength than the former ones resulting in strength degradation of the specimen. Fig. 9 shows that the higher axial compression or the larger cyclic lateral displacement caused steel wall buckling earlier, so the more significant pinching effect was found. It results in shear strength, lateral stiffness, and energy dissipation reduction of the CFST columns as discussed in the next

sections.

3.3 Cyclic envelope, strength and deformation capacity

Test results and comparisons of cyclic response envelopes of the four specimens are presented in Table 3 and Fig. 10. In which, V_{max} and DR_{max} denote maximum shear force and the corresponding interstory drift ratio, respectively. Δ_u and DR_u denote ultimate lateral displacement and ultimate interstory drift ratio, respectively. Herein, Δ_u is defined as the lateral displacement corresponding to the 80% of V_{max} over the peak point, and DR_u is calculated by Δ_u divided to L. For the Specimens CFST42-15C, CFST42-35C and CFST42-55C, the values of V_{max}, Δ_u , and DR_u are average value in positive and negative directions. For the Specimen CFST42-15/55C, these values are the separate values in two directions.

From the analysis results in Table 3 and Fig. 10, some valuable conclusions are drawn as below:

(a) The higher axial compression, the lower shear strength the column had. Comparing to Specimen CFST42-15C, the maximum shear strength (V_{max}) reduction of Specimen CFST42-35C was 7.5% and a large drop was 22.3% in Specimen CFST42-55C. Meanwhile, Specimen CFST42-15/55C reduced about 10.3% and 1% V_{max} in positive (P/P₀ = 0.425) and negative (P/P₀ = 0.275) directions, respectively. Hence, it revealed that when P/P₀ increased from 0.15 to 0.275, V_{max} was almost the same, however, it would be decreased when P/P₀ increased beyond this range. In addition, according to the results of Table 3, the DR_{max} is 2.0, 1.5, 1.0 or 1.5% radian for Specimen CFST42-15C, CFST42-35C, CFST42-55C or CFST42-15/55C, respectively. The conclusion can be made that the higher the axial compression, the lower the DR_{max} corresponding to V_{max}.

(b) Deformation capacity, DR_u or Δ_u , was found significantly different between the four specimens. It revealed that the higher the axial compression, the lower the deformation capacity. The ultimate lateral displacement, Δ_u , or the ultimate interstory drift ratio, DR_u, was used to evaluate the deformation capacity of the columns in this study. From Table 3, it is seen that the highest average DR_u

Table 4 Equivalent viscous damping coefficients and total cumulative energy values

Specimen	ζ_{eq}							E_t (kN-m)
	0.75% (*)	1%	1.5%	2%	3%	4%	5%	
CFST42-15C	-	-	0.145	0.206	0.277	0.315	0.348	2195
CFST42-35C	-	0.085	0.173	0.235	0.375	-	-	1007
CFST42-55C	0.081	0.139	-	-	-	-	-	338
CFST42-15/55C (+)	-	0.075	0.172	0.264	-	-	-	894
CFST42-15/55C (-)	-	0.096	0.181	0.235	0.321	-	-	

(*) Corresponding interstory drift ratio

was 4.92% radian for Specimen CFST42-15C, followed by Specimen CFST42-35C and Specimen CFST42-15/55C in the negative side with DR_u of 3.03% and more than 3.00% radian, respectively. However, Specimen CFST42-15/55C on the positive side had DR_u of 2.34%, and Specimen CFST42-55C showed the lower DR_u of 1.29%, just around one fourth that of Specimen CFST42-15C. In summary, analyzing data shows that in high seismic zones, the CFST column members (B/t equal to 42) subjected to axial compression not exceeding $0.35P_0$ would satisfy the requirement of $DR_u \geq 3.0\%$, a common demand for deformation capacity of columns in the building.

3.4 Shear strength degradation

Peak shear forces at different cycles in the same lateral displacement level of the loading protocol usually reduce due to cumulative damages of constitute materials under cyclic loading. This normally commences after a structural member has already experienced its yield state. The coefficient of shear strength degradation, v_i , is defined by Eq. (1).

$$v_i = V_i^j / V_i^1 \quad (1)$$

where V_i^1 and V_i^j are maximum shear forces in the 1st and j^{th} cycle, respectively, at the cyclic lateral displacement level i^{th} . Values of v_i were calculated at the interstory drift ratio from 1.5% to 5% radian for Specimen CFST42-15C, from 1.5% to 3% radian for Specimens CFST42-35C and CFST42-15/55C, and from 1% to 1.5% radian for Specimen CFST42-55C. This means that v_i equals V_i^4 / V_i^1 and V_i^2 / V_i^1 for displacement level at the drift ratio of 1% and larger displacement levels, respectively. Calculations of v_i were conducted separately in the positive and negative directions.

Results and comparisons of shear strength degradations for four specimens are shown in Fig. 11. According to the results of the columns with the constant axial compressions, shear strength degradation was larger in the direction of negative lateral displacement than in the direction of positive lateral displacement. However, there was a reversal response for Specimen CFST42-15/55C with the varied axial compression. Fig. 11 also reveals that the higher the axial compression or the larger the interstory drift ratio, the steeper the shear strength degradation curve was. For instance, at the interstory drift ratio from 1.0% to 1.5% radian, the shear strength of Specimen CFST42-55C degraded with v_i from 0.883 to 0.762 and from 0.764 to

0.739 in the positive and negative directions, respectively.

Meanwhile, at the drift ratio of 1.5%, v_i slightly varied between 0.973 and 0.994 for three remaining specimens. Moreover, at higher drift ratio levels of 2% and 3% radian, Specimen CFST42-15C kept its shear strength development stable, but Specimens CFST42-35C and CFST42-15/55C showed a significant shear strength degradation, especially for Specimen CFST42-15/55C in the positive direction at +3% with v_i of 0.644.

3.5 Axial stiffness and lateral stiffness degradation

Both axial stiffness and lateral (shear) stiffness of the column play an important role in evaluating the seismic performance of a structure. A theoretical axial elastic stiffness of a composite member, $EA_{Comp.}$, was calculated in this study by the elastic stiffness summation of steel and concrete portions as expressed in Eq. (2).

$$EA_{Comp.} = E_s A_s + E_c A_c \quad (2)$$

where E_s , E_c , and A_s , A_c are elastic moduli and cross-section areas of the steel tube and the concrete infill, respectively. This formula is suitable for short circular CFST columns (Johansson and Gylltoft 2002, Phan and Trinh 2016, de Oliveira *et al.* 2009). However, Eq. (2) is necessary to be evaluated for the square CFST columns with full-scale ones. An experimental axial stiffness of square CFST column ($K_{Exp.-Ax.}$) was defined by averaging axial stiffness values obtained from the four specimens. The values of $K_{Exp.-Ax.}$ and $EA_{Comp.}$ calculated are 9.9414×10^6 kN and 10.9985×10^6 kN, respectively, and then $K_{Exp.-Ax.}/EA_{Comp.} = 0.904$. It shows that Eq. (2) overestimated the axial elastic stiffness of the columns in this study. Hence, the authors propose a modified formula by multiplying the right-hand side of Eq. (2) with a reduction coefficient of 0.9, to predict more reasonably the axial elastic stiffness of square CFST columns.

A lateral (secant) stiffness at a cyclic lateral displacement level i^{th} (K_i) of the CFST column was defined by Eq. (3), where i is the sequential number of lateral displacement levels in the loading protocol, according to the definition of secant stiffness in the AISC 360 (2016) code and the application in Zhang *et al.*'s (2007) study.

$$K_i = \sum_{j=1}^n (V_i^{j+} - V_i^{j-}) / \sum_{j=1}^n (\Delta_i^{j+} - \Delta_i^{j-}) \quad (3)$$

where V_i^{j+} , V_i^{j-} and Δ_i^{j+} , Δ_i^{j-} are peak shear force and peak lateral displacement in the j^{th} cycle at cyclic lateral

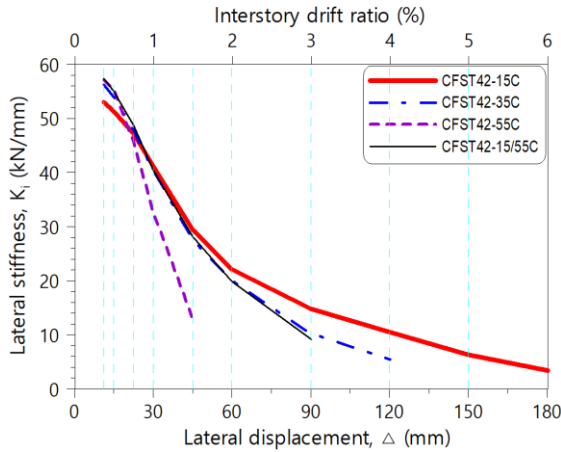


Fig. 12 Comparisons of lateral stiffness degradation

displacement level i^{th} in the positive and negative directions, respectively; and n is a total number of cycles tested at the corresponding displacement level i^{th} .

The comparisons of lateral stiffness degradations during the seismic testing for all four specimens are presented in Fig. 12. Generally, the higher the axial compression, the larger the initial lateral stiffness obtained, but the faster the lateral stiffness degradation happened. For instance, at the interstory drift ratio of 1.5% radian, the lateral stiffness of Specimens CFST42-15C, CFST42-35C and CFST42-55C were 29.44, 27.59 and 13.05 kN/mm, respectively. Another interesting finding was that at smaller interstory drift ratios from 0.375% to 1.5% radian, the lateral stiffness of Specimen CFST42-15/55C was always higher than that of Specimen CFST42-35C. However, at larger interstory drift ratios (2% and 3% radian), the lateral stiffness of Specimen CFST42-35C dominated.

3.6 Energy dissipation

The energy dissipation capacity is one of the key indices to evaluate the seismic performance of a column member. High energy dissipation capacity discloses its good seismic behavior. In this study, two methods were used to estimate energy dissipation, namely the equivalent viscous damping coefficient (ζ_{eq}) and total cumulative energy (E_t). The first method is to calculate ζ_{eq} defined in Eq. (4) (Chopra, 2012).

$$\zeta_{eq} = E_D / (4\pi E_{So}) \quad (4)$$

where E_D is the dissipating energy in the column that is the elliptic hysteresis loop area (AECFG), and E_{So} is the strain energy calculated by the average area of the triangles OAB and OCD as depicted in Fig. 13. The second method is to compute cumulative dissipating energy dissipation in all hysteresis loops. Values of ζ_{eq} at various interstory drift ratios (beyond yield state) and E_t of the four specimens were presented in Table 4.

Table 4 shows that the larger the interstory drift ratio, the higher the ζ_{eq} obtained, while the final ζ_{eq} (before fracture state) of all specimens ranges from 0.139 to 0.375. This reveals that generally, the CFST columns in this research had better energy dissipation capacity compared to

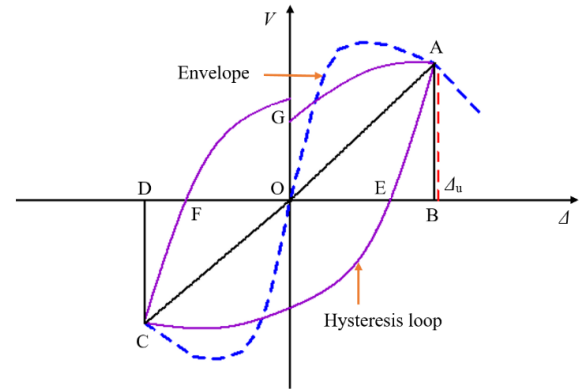
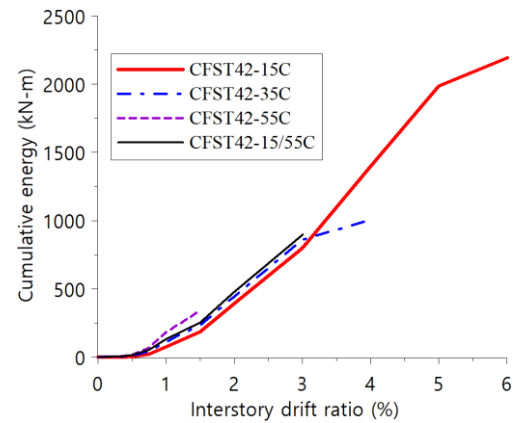
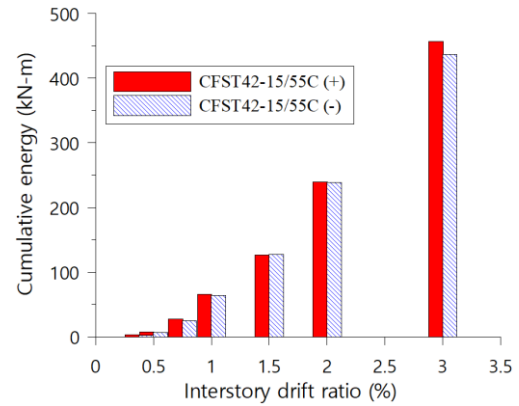


Fig. 13 Defining the equivalent viscous damping coefficient



(a) Comparison of cumulative dissipating energy



(b) Cumulative dissipating energy of Specimen CFST42-15/55C

Fig. 14 Quantitative comparisons of dissipating energy

the RC columns with the final ζ_{eq} ranging between 0.1 and 0.2 (Calvi *et al.* 2007). The analysis data in Table 4 shows that only Specimen CFST42-55C had a low final ζ_{eq} of 0.139 that falls into the common range of RC columns. The three remaining specimens presented a better energy dissipation capacity with ζ_{eq} beyond the RC column range at an interstory drift ratio that is more than or equal to 2% radian. Specimen CFST42-35C had the highest final ζ_{eq} , followed by Specimen CFST42-15C and Specimen CFST42-15/55C in the negative and positive directions, respectively.

Fig. 14 shows a quantitative comparison of the energy dissipation capacities of the four specimens and another

comparison for Specimen CFST42-15/55C in positive and negative directions. From Fig. 14(a), it was shown that the lower the axial compression, the larger the total cumulative energy obtained. For instance, E_t of Specimen CFST42-15C was nearly 2.2 and 6.5 times that of Specimens CFST42-35C and CFST42-55C, respectively. Meanwhile, E_t of Specimen CFST42-15/55C was around 89% of Specimen's CFST42-35C. Another finding was that, at the same interstory drift ratio, the specimen under higher axial compression had larger cumulative energy. Besides, for Specimen CFST42-15/55C, E_t (+) was 20 kN-m higher than E_t (-) at the drift ratio of 3% radian (Fig. 14(b)).

4. Conclusions

Based on the analyses and comparisons of experimental results between the four full-scale square CFST column specimens in this study, the following conclusions were drawn:

- The axial compression levels directly influenced the seismic behavior and performance of the CFST columns. The largest hysteresis loop, up to an interstory drift ratio of 6% radian, was obtained from Specimen CFST42-15C with the lowest axial compression ($0.15P_0$). In contrast, the smallest hysteresis loop, up to 1.5% radian, was obtained in the case of the highest axial compression of $0.55P_0$ from Specimen CFST42-55C. For the rest of the axial compression levels (0.2 – $0.5P_0$), the hysteresis loops between 3 and 4% were obtained.
- The shear strength and deformation capacity were minimized when the axial compression was increased from 0.35 to $0.55P_0$. When the axial compression was more than $0.35P_0$, the deformation capacity was less than 3% radian. This could not satisfy a common seismic deformation demand of 3% radian for the building column members. When the axial compression increased from 0.15 to $0.275P_0$, the deformation capacity was proportionally reduced but the shear strength seemed to remain unchanged.
- The specimen with high axial compression led to the shear strength more stable before reaching its maximum shear than that with low axial compression. However, the higher the axial compression, the earlier and faster the (post-peak) shear strength degradation occurred. Also, the raises of axial compression harmed to shear strength development.
- The axial compression level and the cyclic loading had certain effects on the lateral stiffness of the column. A higher axial compression created a larger lateral stiffness initially. By contrast, in the next lateral loading steps, the higher axial compression resulted in faster degradation of the lateral stiffness. Additionally, it was found that the theoretical axial stiffness obtained from Eq. (2) overestimated 10% of the axial stiffness of the square CFST columns in this study.
- The CFST columns exhibited better energy dissipation capacity ($\xi_{eq} > 0.2$) compared to that of RC columns under axial compression less than or equal to $0.425P_0$. Test results revealed that with lower axial compression,

the total cumulative energy was higher. Nonetheless, at the same deformation level, the higher the axial compression, the larger the cumulative energy obtained.

• B/t requirements in current codes (AISC 360 2016, ACI 318 2014, AIJ 2008, EC4 2004) cannot provide sufficient seismic performance for square CFST columns having high axial compression ($> 0.35P_0$) in high seismic zones. However, based on the limited evidence from this research, the B/t limit required in the ACI 318 (2014) code only satisfies the seismic design of CFST columns in the case of low or medium axial compression ($\leq 0.35P_0$). Alternatively, another performance-based design way may be recommended that under an identical seismic demand, specifying different B/t limits depend upon different axial compression levels instead of one particular B/t limit. Moreover, delaying or preventing the steel tube from the occurrence of local buckling is a fundamental measure to sufficiently develop the earthquake resistance capacity or reduce the pinching effect for CFST columns.

Acknowledgments

The authors greatly appreciate the financial support provided by the National Center for Research on Earthquake Engineering (NCREE), Taiwan. The authors also would like to send many thanks to the staff and technicians of NCREE for their enthusiastic supports and hard efforts as well.

References

- Uy, B. (1998), "Concrete-filled fabricated steel box columns for multistorey buildings: behaviour and design", *Prog. Struct. Eng. Mat.*, **1**(2), 150-158. <https://doi.org/10.1002/pse.2260010207>.
- Boyd, P.F., Cofer, W.F. and Mclean, D.I. (1995), "Seismic performance of steel-encased concrete columns under flexural loading", *ACI Struct. J.*, **92**(3), 355-364.
- Fam, A., Qie, F.S. and Rizkalla, S. (2004), "Concrete-filled steel tubes subjected to axial compression and lateral cyclic loads", *J. Struct. Eng.*, **130**(4), 631-640. [https://doi.org/10.1061/\(ASCE\)0733-9445\(2004\)130:4\(631\)](https://doi.org/10.1061/(ASCE)0733-9445(2004)130:4(631)).
- Han, L.H., Yang, Y.F. and Tao, Z. (2003), "Concrete-filled thin-walled steel SHS and RHS beam-columns subjected to cyclic loading", *Thin Walled Struct.*, **41**(9), 801-833. [https://doi.org/10.1061/\(ASCE\)0733-9445\(2004\)130:4\(631\)](https://doi.org/10.1061/(ASCE)0733-9445(2004)130:4(631)).
- Fujimoto, T., Mukai, A., Nishiyama, I. and Sakino, K. (2004), "Behavior of eccentrically loaded concrete-filled steel tubular columns", *J. Struct. Eng.*, **130**(2), 203-212. [https://doi.org/10.1061/\(ASCE\)0733-9445\(2004\)130:2\(203\)](https://doi.org/10.1061/(ASCE)0733-9445(2004)130:2(203)).
- Inai, E., Mukai, A., Kai, M., Tokinoya, H., Fukumoto, T. and Mori, K. (2004), "Behavior of concrete-filled steel tube beam columns", *J. Struct. Eng.*, **130**(2), 189-202. [https://doi.org/10.1061/\(ASCE\)0733-9445\(2004\)130:2\(189\)](https://doi.org/10.1061/(ASCE)0733-9445(2004)130:2(189)).
- Varma, A.H., Ricles, J.M., Sause, R. and Lu, L.W. (2002a), "Experimental behavior of high strength square concrete-filled steel tube beam-columns", *J. Struct. Eng.*, **128**(3), 309-318. [https://doi.org/10.1061/\(ASCE\)0733-9445\(2002\)128:3\(309\)](https://doi.org/10.1061/(ASCE)0733-9445(2002)128:3(309)).
- Varma, A.H., Ricles, J.M., Sause, R. and Lu, L.W. (2002b), "Seismic behavior and modeling of high-strength composite concrete-filled steel tube (CFT) beam-columns", *J. Construct.*

- Steel Res.*, **58**(5-8), 725-758. [https://doi.org/10.1016/S0143-974X\(01\)00099-2](https://doi.org/10.1016/S0143-974X(01)00099-2).
- Varma, A.H., Ricles, J.M., Sause, R. and Lu, L.W. (2004), "Seismic behavior and design of high-strength square concrete-filled steel tube beam columns", *J. Struct. Eng.*, **130**(2), 169-179. [https://doi.org/10.1016/S0143-974X\(01\)00099-2](https://doi.org/10.1016/S0143-974X(01)00099-2).
- Varma, A.H., Sause, R., Ricles, J.M. and Li, Q. (2005), "Development and validation of fiber model for high-strength square concrete-filled steel tube beam-columns", *ACI Struct. J. Amer. Concrete Institute*, **102**(1), 73-84.
- AISC 360 (2016), "Specification for structural steel buildings", American Institute of Steel Construction; Chicago, U.S.A.
- ACI 318 (2014), "Building code requirements for structural concrete and commentary", American Concrete Institute; Farmington Hills, U.S.A.
- AIJ (2008), "Recommendations for design and construction of concrete filled steel tubular structures", Architectural Institute of Japan.
- Eurocode (EC) 4 (2004), "Design of composite steel and concrete structures - Part 1-1: General rules and rules for buildings", European Committee for Standardization; Brussels, Belgium.
- AISC 341 (2016), "Seismic provisions for structural steel buildings", American Institute of Steel Construction; Chicago, U.S.A.
- Eurocode (EC) 8 (2004), "Design of structures for earthquake resistance - Part 1: General rules, seismic actions and rules for buildings", European Committee for Standardization; Brussels, Belgium.
- Thai, S., Thai, H.T., Uy, B. and Ngo, T. (2019), "Concrete-filled steel tubular columns: Test database, design and calibration", *J. Construct. Steel Res.*, **157**, 161-181. <https://doi.org/10.1016/j.jcsr.2019.02.024>.
- AASHTO (2008), "Standard test methods for tension testing of metallic materials (E8/E8M-08)", American Association State Highway and Transportation Officials, West Conshohocken, U.S.A.
- Zhang, Y., Xu, C. and Lu, X. (2007), "Experimental study of hysteretic behaviour for concrete-filled square thin-walled steel tubular columns", *J. Construct. Steel Res.*, **63**(3), 317-325. <https://doi.org/10.1016/j.jcsr.2006.04.014>.
- Johansson, M. and Gylltoft, K. (2002), "Mechanical behavior of circular steel-concrete composite stub columns", *J. Struct. Eng.*, **128**(8), 1073-1081. [https://doi.org/10.1061/\(ASCE\)0733-9445\(2002\)128:8\(1073\)](https://doi.org/10.1061/(ASCE)0733-9445(2002)128:8(1073)).
- Phan, H.D. and Trinh, H.H. (2016), "Analysis of mechanical behaviour of circular concrete filled steel tube columns using high strength concrete", *The Proceedings of the 24th Australian Conference on the Mechanics of Structures and Materials*, Perth, Australia, December.
- de Oliveira, W.L.A., Nardin, S.D., de Cresce El Debs, A.L.H. and Debs, M.K.E. (2009), "Influence of concrete strength and length/diameter on the axial capacity of CFT columns", *J. Construct. Steel Res.*, **65**(12), 2103-2110. <https://doi.org/10.1016/j.jcsr.2009.07.004>.
- Chopra, A.K. (2012), "Dynamics of Structures: Theory and Applications to Earthquake Engineering", Prentice Hall, Upper Saddle River, U.S.A.
- Calvi, G.M., Priestley, M.J.N. and Kowalsky, M.J. (2007), "Displacement-based seismic design of structures", *The Proceedings of the New Zealand Conference on Earthquake Engineering*, Wellington, New Zealand, November.